Bead Optimization And Metallurgical Analysis Of Claddings Produced With Recycled Slag In Submerged Arc Welding

Navneet Goyal [1*], Kulwant Singh [2]

[1,2]Department of Mechanical Engineering, SLIET, Longowal, Sangrur, Punjab 148106, India
[*]corresponding author e-mail: navneet6234@gmail.com

Abstract

The waste slag which is by-product of steel plant has been recycled as a cladding flux for submerged arc welding (SAW). The recycled slag is applied as a flux in SAW for stainless steel cladding. The bead profile in terms of penetration, width of bead and reinforcement have been investigated and compared with that of original fresh flux. The experiments were performed using central composite design of experiments technique and optimization was achieved with RSM, to improve the performance of claddings. It observed that recycled slag has produced weld profile at par with that of virgin flux. The weld penetration, width of bead and reinforcement obtained using recycled slag is 5.25, 15.11 and 3.98 mm, respectively, which is comparable to that of equivalent virgin flux (5.35, 15.22 and 3.87 mm). The width of bead decreased from 11.0 to 8.2 mm as travel speed is increased from 8 to 34 m/hr. The penetration decreased from 7.4 to 5.9 mm, by increasing travel speed from 18 to 34 m/hr. The optimized parameters obtained are: welding current 427 amperes, travel speed 34 m/hr, voltage 34 volts. It is further observed that recycled slag has yielded desirable microstructure having skeletal delta ferrite embedded within austenitic matrix. The compounds formed within microstructure are also compables. This research is a step forward towards 'waste to wealth' technology for circular economy.

Keywords: Slag, flux, cladding, penetration, weld width, reinforcement.

1. Introduction:

Submerged arc welding (SAW) is a widely used in heavy industries, where a granular fusible flux, typically derived from minerals mined from the earth's crust, is used to shield the molten pool. However, the continuous extraction of these minerals is depleting natural resources at an alarming rate. Simultaneously, steel slag, a byproduct of steel manufacturing, is often discarded as waste, contributing to soil, water, and air pollution. Globally, the annual production of steel slag is approximately 1814 million tonnes (MT) [1], with India generating around 19 MT and the United States producing about 290 MT annually [2,3]. In response to growing environmental concerns, researchers, engineers, and technologists are striving to develop sustainable methods to reduce, reuse, and recycle steel slag. Steel slag has already been successfully repurposed in several industries. It has been widely used in road construction and civil engineering projects. while Liu et al. [4] reported that incorporating steel slag powder into cement concrete mixtures enhances fluidity, improving workability. Additionally, its silicon content has been found to promote plant growth, making it a viable raw material for agricultural fertilizers [5]. In the foundry industry, powdered steel slag mixed with silica sand has been successfully used for mold making [6,7].

The feasibility of reusing SAW slag as a flux has been demonstrated by Nimker et al. [8]. while Garg et al [9,10] confirmed its suitability for both welding and cladding applications. Further, Saini et al. [11] explored the possibility of recycling waste steel slag into welding flux and reported that the resulting weld chemistry complies with ASME specifications [12]. Inspite of these advancements, a notable gap has been observed in the literature regarding the use of steel slag as a flux specifically for stainless steel cladding in the SAW process.

In their earlier study, the authors successfully recycled steel slag into a SAW flux for stainless steel cladding [13]. Weld profile plays a critical role in the integrity and performance of cladded surfaces, as deviations can lead to defects such as lack of fusion and incomplete penetration. Additionally, the width of the cladding layer determines the minimum number of passes required for complete substrate coverage, while optimal penetration ensures a strong metallurgical bond, preventing delamination and enhancing durability. Therefore, understanding the dynamic relationship between welding variables and weld profile is essential for optimizing the performance of a recycled steel slag-based flux.
The present research investigates the effects of welding varialbles on the bead geometry of the cladding layer using recycled steel slag as a flux. A Central Composite Design (CCD) approach was employed to conduct experiments and analyze the effect of welding variables on weld profile. Additionally, the study compares the bead geometry and microstructural characteristics of clads deposited using recycled steel slag with those produced using fresh flux. By integrating process optimization, microstructural analysis, and environmental considerations, this research aims to enhance the efficiency, reliability, and sustainability of cladding operations. The performance of recycled slag regarding bead geometry, microstructure and phase formation has been investigated. The process variables have been optimized to get favourable bead geometry.

2. Materials and methods

2.1 Transformation of steel slag into cladding flux

The reclamation of slag is a meticulously structured process that unfolds in successive stages, involving the collection, crushing, and palletisation of slag until it attains a grain size akin to that of welding flux, rendering it fit for welding purpose. Additionally, this methodology incorporates a comparative study that scrutinizes the differences between performance of virgin flux and recycled slag, verifying the composition of various additives utilized in the recycling process. The slag utilized in this research was taken at no cost from a disposal site of steel producing plant, where it was dumped as a waste material. This slag underwent a series of transformative steps to become a valuable material. Initially, it was subjected to mechanical crushing followed by milling to convert it into fine powder using a ball mill. To ensure its performance for intended application, alloying elements and deoxidizers were incorporated into the powdered slag. The mixture was thoroughly homogenized in a ball mill for half an hour to ensure even distribution of these elements.To shape and consolidate the mixture, a liquid potassium silicate binder was introduced. Subsequently, the damp mixture was passed through a sieve with a 2 mm mesh, leading to the formation of pellets. These newly formed pellets were dried in air for 20 hours to remove any excess moisture, rendering them ready for the next stage.

After the drying process, the pellets were baked at 800°C for duration of 3 hours within a muffle furnace. This step known as sintering, significantly contributed to the material's strength and structural transformation. The sintered mass was crushed and then sieved to obtain desired grain size and reffered as ‘recycled steel slag’. This recycled slag was applied as a flux for further investigations.

2.2 Mathematical modelling of bead geometry

To develop mathematical models for key bead geometry elements namely width of weld (w), depth of penetration (p), and height of reinforcement (r) of the cladding layer deposited using recycled steel slag (Fig. 1), experiments were performed as dictated by Central Composite Design (CCD) methodology. The welding variables considered were: welding current (I), travel speed (S), arc voltage (V), and nozzle-to-plate distance (N). Design Expert software version 13 was used to design the experiments and to develop the relationships among these parameters and weld geometry characteristics.

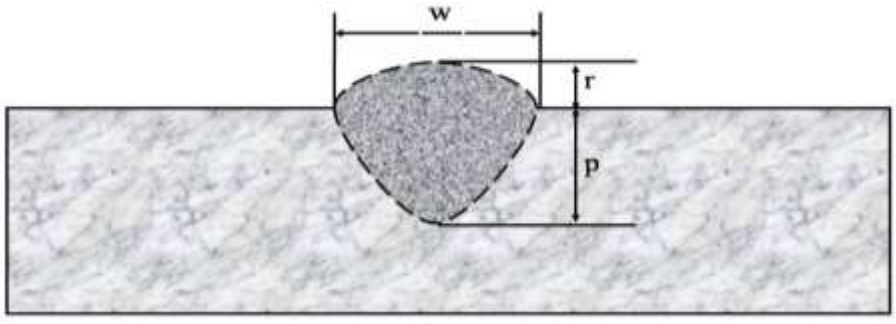

Figure 1. Elements of weld profile

Extensive experimental trials were conducted to determine the welding parameters and their operational limits. During preliminary investigations, welding current, welding speed, and nozzle-to-plate distance (NPD) were identified as the most influential factors affecting the weld profile. To facilitate identification and calculation, the parameter values were assigned coded levels: the middle value was designated as (0), the lower and lowest values as (-1) and (-2), respectively, while the higher and highest values were represented as (+1) and (+2). The specific parameter values and their corresponding levels are summarized in Table 1.

Table 1: Selected welding parameters

			Working range				
Parameters	**Units**	**Symbols**	**−2**	**−1**	**0**	**+1**	**+2**
Welding current	Ampere	I	225	325	425	525	625
Weldingspeed	m/h	S	18	22	26	30	34
Voltage	Volts	V	22	25	28	31	34
NPD	mm	N	20	22	24	26	28

In this study, four welding parameters were considered at five levels each. The Central Composite Design (CCD) technique generated a design matrix consisting of 31 experiments, including 16 factorial, 8 star, and 7 center points. The complete design matrix, as determined by the CCD method, along with the corresponding experimental outputs, is presented in Table 2.

A total of 31 experiments were conducted in accordance with the design matrix. The weld bead deposits were produced using a submerged arc welding (SAW) machine (Tornado SAW M 800). The substrate material used was SA 516 Grade 70, with dimensions of 12×75×120 mm length. This material was chosen due to its widespread application in the construction of boilers, pressure vessels, and heat exchangers [14]. A SS 308L wire electrode was used for cladding, in combination with the recycled steel slag flux.

Table 2: Design matrix and responses

	Process parameters				**Response variables (mm)**		
S. No.	**I**	**S**	**V**	**N**	**p**	**w**	**r**
1	−1	−1	−1	−1	9.42	7.5	5.155
2	1	−1	−1	−1	6.3	15.5	4.105
3	−1	1	−1	−1	6.9	7.1	6.725
4	1	1	−1	−1	5.2	12.1	3.153
5	−1	−1	1	−1	6.2	7.2	6.25
6	1	−1	1	−1	8.5	6.7	6.845
7	−1	1	1	−1	7.5	9.1	6.814
8	1	1	1	−1	6.3	11.2	4.235
9	−1	−1	−1	1	7.1	11.8	6.753
10	1	−1	−1	1	8	9.8	5.275
11	−1	1	−1	1	8.7	7.8	6.745
12	1	1	−1	1	5.4	15.1	3.475
13	−1	−1	1	1	10.5	14.4	4.407
14	1	−1	1	1	8.5	10.5	3.147
15	−1	1	1	1	8.2	8.8	6.142

16	1	1	1	1	5.5	6.5	5.925
17	−2	0	0	0	8.1	7.2	6.258
18	2	0	0	0	6.15	8.9	5.125
19	0	−2	0	0	8.5	9.5	5.114
20	0	2	0	0	4.15	11.5	2.478
21	0	0	−2	0	6.14	8.8	5.514
22	0	0	2	0	4.9	8.5	6.175
23	0	0	0	−2	9.5	8.1	5.355
24	0	0	0	2	5.9	17.5	4.235
25	0	0	0	0	8.1	7.1	6.189
26	0	0	0	0	6	8.8	6.757
27	0	0	0	0	8.12	7.6	6.324
28	0	0	0	0	4.5	13.5	2.835
29	0	0	0	0	8.2	7.2	6.225
30	0	0	0	0	9.1	10.2	6.021
31	0	0	0	0	7.1	7	5.175

To analyze the weld bead geometry, a 15 mm wide sample was cut from the middle of each deposited bead. The samples were polished using different grades of emery paper and then etched with Carpenter's etchant [13]. After etching, bead dimensions were measured with the help of 'ImageJ' software. The weld dimensions are given in Table 2.

2.2.1Model for penetration

Response Surface Methodology (RSM) was employed to develop models which could be used for prediction of bead geometry characteristics. To assess the influence of parameters on the responses, Analysis of Variance (ANOVA) was conducted. The ANOVA results indicate that the model for penetration is significant, as the 'p-value' is less than 0.05.

Table 3: ANOVA for penetration

Source	**Sum of Squares**	**DOF**	**Mean**	**F-value**	**p-value**		Contribution (%)
Model	2.70	14	0.1931	38.37	< 0.0001	significant	
I	1.38	1	1.38	273.85	< 0.0001		51.11
S	0.0973	1	0.0973	19.34	0.0004		3.60
V	0.0651	1	0.0651	12.93	0.0024		2.41
N	0.0820	1	0.0820	16.29	0.0010		3.03
IS	0.0225	1	0.0225	4.47	0.0505	Non-significant	0.83
IV	0.2495	1	0.2495	49.59	< 0.0001		9.24
IN	0.0493	1	0.0493	9.79	0.0065		1.82
SV	0.0231	1	0.0231	4.59	0.0479		0.85
SN	0.0009	1	0.0009	0.1812	0.6760	Non-significant	0.03
VN	0.0203	1	0.0203	4.04	0.0615	Non-significant	0.75
I^2	0.1570	1	0.1570	31.20	< 0.0001		5.81
S^2	0.1450	1	0.1450	28.81	< 0.0001		5.37

V^2	0.5111	1	0.5111	101.58	< 0.0001		18.92
N^2	0.0005	1	0.0005	0.0898	0.7683	Non-significant	0.01
Residual	0.0805	16	0.0050				
Lack of Fit	0.0707	10	0.0071	4.34	0.0528	Non-significant	
Pure Error	0.0098	6	0.0016				
Cor Total	2.78	30					
Standard Deviation = 0.0709			**R^2** = 0.9711		**Adjusted R^2** = 0.9458		
Mean = 2.66					**Predicted R^2** = 0.84.89		

Furthermore, both individual factors (I, S, V, and N) and interaction effects (IV, IN, and SV) were found to have a significant influence on penetration. The model was determined as highly adequate, with (R^2) of 97.11%, confirming its reliability in predicting penetration behavior. The contribution percentage of welding parameters to penetration is summarized in Table 3. The mathematical equation developed using the significant terms is presented in Equation 1.

2.2.2 Model for width of bead

The mathematical model developed using significant coefficients is presented in Equation 2, while the ANOVA results for bead width are summarized in Table 4. The ANOVA analysis confirms that the model is statistically significant, because 'p-value' is less than 0.05.

The model highlights that individual factors (I, S, and V) as well as interaction effects (IS, IV, SV, and SN) significantly influence bead width. Additionally, the model's adequacy is demonstrated by a coefficient of determination (R^2) of 95.2%, confirming its reliability in predicting bead width variations.

Table 4: ANOVA for width of bead

Source	**Sum of Squares**	**DOF**	**Mean**	**F-value**	**p-value**		**Contribution (%)**
Model	5.64	14	0.4026	22.69	< 0.0001	significant	
I	0.5180	1	0.5180	29.19	< 0.0001		9.18
S	0.1470	1	0.1470	8.28	0.0109		2.60
V	2.24	1	2.24	126.28	< 0.0001		39.71
NPD	1.827E-07	1	1.827E-07	0.0000	0.9975	Non-significant	.003
IS	0.2013	1	0.2013	11.35	0.0039		3.56
IV	0.2571	1	0.2571	14.49	0.0016		4.55
IN	0.0704	1	0.0704	3.97	0.0637	Non significant	1.24
SV	0.5134	1	0.5134	28.93	< 0.0001		9.140
SN	0.2740	1	0.2740	15.44	0.0012		4.85
VN	0.0209	1	0.0209	1.18	0.2936	Non significant	0.37
I^2	0.1822	1	0.1822	10.27	0.0055		3.23
S^2	0.2881	1	0.2881	16.23	0.0010		5.10
V^2	1.01	1	1.01	56.66	< 0.0001		17.90
N^2	0.2664	1	0.2664	15.01	0.0013		4.2
Residual	**0.2839**	**16**	**0.0177**				
Lack of Fit	**0.1947**	**10**	**0.0195**	**1.31**	**0.3852**	**not significant**	
Pure Error	**0.0892**	**6**	**0.0149**				

Cor Total	**5.92**	**30**		
Standard Deviation = 0.1332		**R² = 0.9520**	**Adjusted R² = 0.9101**	
Mean = 3.09			**Predicted R² = 0.7900**	

2.2.6 Model for reinforcement

The ANOVA for reinforcement is presented in Table 5, indicating that the model is statistically significant, as 'p-value' is less than 0.05. The analysis further reveals that individual factors (I, S, V, and N) and interaction effects (IS, IV, and IN) have a significant influence on reinforcement.

The model demonstrates a high level of adequacy, with a coefficient of determination (R^2) of 96.69%, confirming its reliability in predicting reinforcement behavior. The mathematical model developed based on the ANOVA results is provided in Equation 3.

Table 5: ANOVA for reinforcement

Source	**Sum of Squares**	**DOF**	**Mean**	**F-value**	**p-value**		Contribution (%)
Model	2.65	14	0.1892	33.38	< 0.0001	significant	
I	0.6791	1	0.6791	119.81	< 0.0001		25.62
S	0.0597	1	0.0597	10.53	0.0051		2.25
V	0.3890	1	0.3890	68.63	< 0.0001		14.67
NPD	0.1671	1	0.1671	29.47	< 0.0001		6.30
IS	0.1209	1	0.1209	21.32	0.0003		4.56
IV	0.1622	1	0.1622	28.62	< 0.0001		6.12
IN	0.1903	1	0.1903	33.57	< 0.0001		7.18
SV	0.0150	1	0.0150	2.64	0.1234	Non-significant	0.56
SN	0.0031	1	0.0031	0.5515	0.4685	Non-significant	0.11
VN	0.0004	1	0.0004	0.0634	0.8044	Non-significant	0.01
I^2	0.5345	1	0.5345	94.29	< 0.0001		20.16
S^2	0.0006	1	0.0006	0.0971	0.7594	Non-significant	0.02
V^2	0.0861	1	0.0861	15.20	0.0013		3.25
N^2	0.3710	1	0.3710	65.45	< 0.0001		14.00
Residual	0.0907	16	0.0057				
Lack of Fit	0.0721	10	0.0072	2.32	0.1573	Non-significant	
Pure error	0.0186	6	0.0031				
Cor Total	2.74	30					
Standard Deviation = 0.0753		**R² =** 0.9669		**Adjusted R²** = 0.9379			
Mean = 2.29				**Predicted R²** = 0.8392			

3. Results and Discussions

3.1 Influence of welding parameters on weld geometry

3.1.1 The effect of welding variables on penetration

The mathematical model for penetration is presented in Eq. 1. To provide a clearer understanding of the effect of parameters on penetration, Fig. 2(a–d) illustrates their graphical representation. The trends observed in these figures offer insights into the relationship between process parameters and penetration depth, facilitating a comprehensive analysis.

$$\mathbf{p} = 2.88 + 0.2396\mathrm{I} - 0.0637\mathrm{S} + 0.0521\mathrm{V} - 0.0584\mathrm{N} + 0.1249\mathrm{IV} - 0.0555\mathrm{IN} - 0.0380\mathrm{SV} - 0.0741\mathrm{I}^2 - 0.0712\mathrm{S}^2 - 0.1337\mathrm{V}^2 \quad (1)$$

Both the mathematical model and Fig. 2(a) indicate that penetration increases with rising welding current. Specifically, when the welding current increases from 225 to 625 A, while keeping all other parameters constant, the penetration depth rises from 3 to 9 mm. This can be attributed to the higher heat input, which enlarges the molten pool, resulting in greater penetration and bead width. Additionally, the higher current density enhances the arc's digging power, further contributing to deeper penetration. Similar trends have been found by Shakya et al [15].

Fig. 2(b) illustrates the effect of travel speed on penetration. As travel speed increases from 18 m/hr to 34 m/hr, penetration decreases from 6.8 mm to 5.8 mm. This reduction occurs due to the lower heat input at higher travel speeds, which leads to a smaller molten pool and consequently reduced penetration [16].

The influence of arc voltage on penetration is shown in Fig. 2(c). An increase in voltage from 22 V to 34 V results in a rise in penetration from 5 mm to 6.3 mm. This behavior is attributed to the increased heat input associated with higher arc voltage, which enhances molten pool formation and promotes deeper penetration.

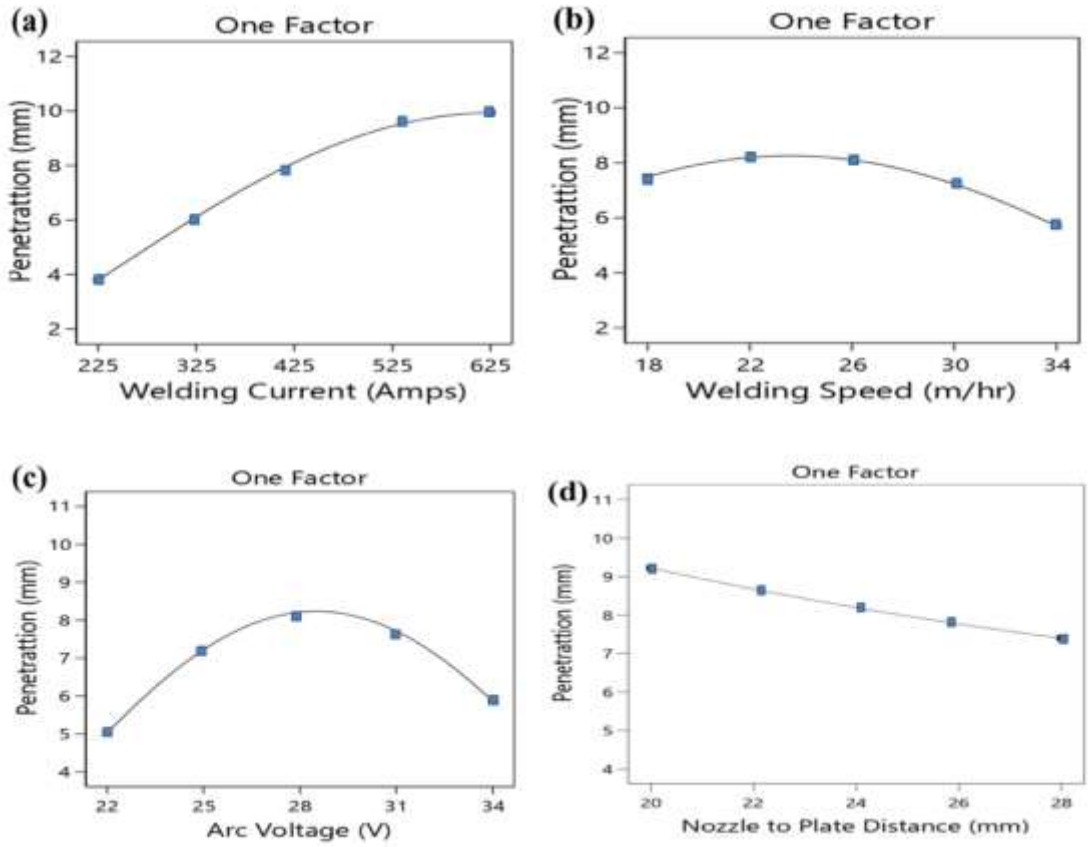

Figure 2: Effect of (a) welding current(b) travel speed (c) arc voltage (d)NPD on penetration.

Finally, Fig. 2(d) illustrates the effect of NPD on penetration. As the NPD increases, penetration decreases. This reduction is attributed to the larger arc gap, which causes the arc to disperse over a wider surface area, leading to diminished penetration and increased bead width.

3.1.2 Effect of variables on bead width

The mathematical model for bead width is presented in Eq. 2, and the effect of various welding variables on bead width is graphically illustrated in Fig. 3(a–d).

$$w = 2.73 - 0.1469I - 0.0783S + 0.3056V - 0.1122IS - 0.1268IV - 0.1791SV + 0.1309SN + 0.0798I^2 + 0.1004S^2 + 0.1875V^2 + 0.0965N^2 \quad (2)$$

Fig. 3(a) illustrates that bead width decreases from 11.2 mm to 8 mm as welding current increases from 225 A to 625 A. This trend can be explained by Stenbeck's principle, which states that an increase in current leads to arc constriction. A constricted arc impinges on a smaller surface area, thereby reducing width of weld.

Similarly, Fig. 3(b) illustrate, bead width decreases from 11 to 9 mm when travel speed increased from 18 m/hr to 34 m/hr. Higher travel speeds reduce the heat input to the work surface, leading to a smaller molten pool and, consequently, reduced penetration and bead width. These observations are consistent with findings from previous studies [17].

Conversely, Fig. 3(c) demonstrates that width of bead enhanced from 8.1 to 16 mm as voltage rises from 22 V to 34 V. This behavior is attributed to the increased arc gap, which causes the arc to spread over a larger surface area, thereby widening the weld bead.Finally, Fig. 3(d) indicates that nozzle-to-plate distance has only a marginal impact on bead width.

These investigations act as light house for welding engineers to select optimal vlue of variable to achieve desired bead profile which is crucial for achieving the desired weld quality.

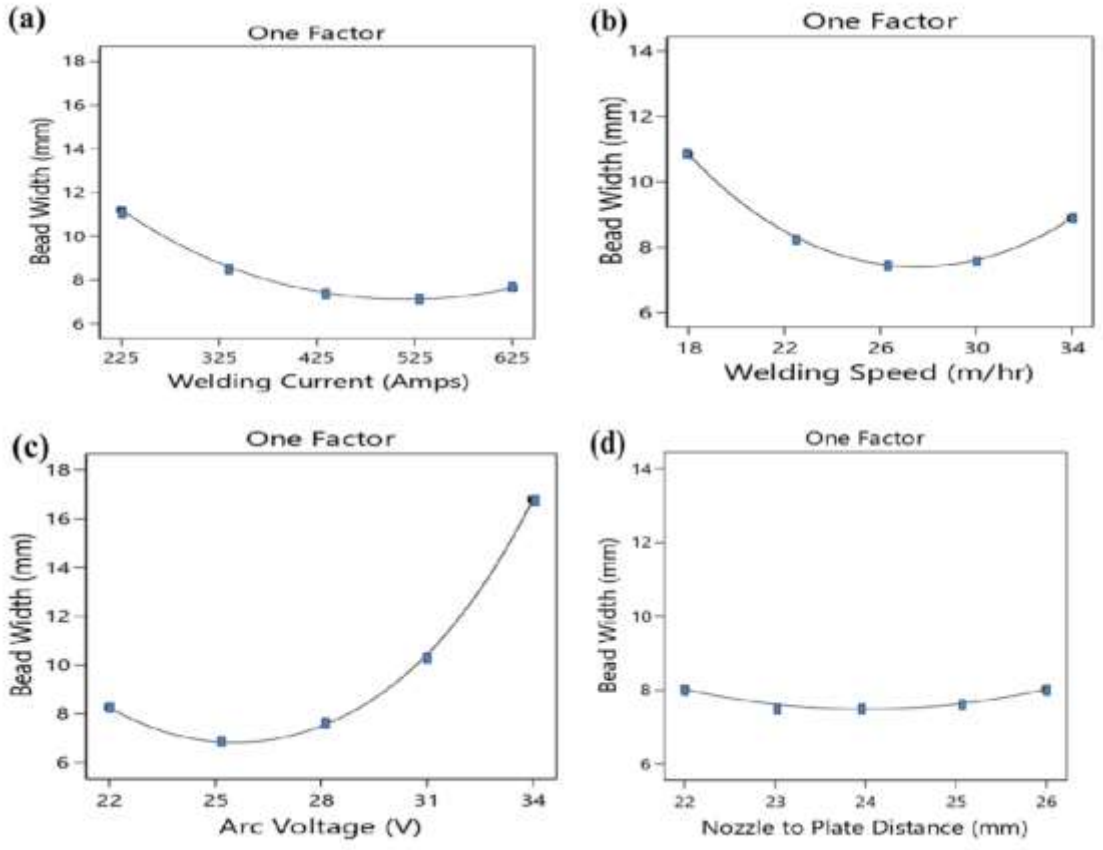

Figure 3:Effect of (a) current (b) welding speed (c) voltage (d) NPD on bead width

3.1.3 Influence of parameters on reinforcement

The model developed for reinforcement is presented in Eq. 3, and effect of variables is graphically illustrated in Fig. 4 (a–d).

$$r = 2.53 + 0.1682I - 0.0499S - 0.1273V + 0.0834N + 0.0869IS + 0.1007IV + 0.1090IN - 0.1367I^2 - 0.0549V^2 - 0.1139N^2 \quad (3)$$

As shown in Fig. 4(a), reinforcement increases from 2.7 mm to 5.3 mm as welding current rises from 225 A to 625 A. This increase is attributed to a higher melting rate at elevated currents, which results in greater reinforcement. These findings align well with those reported by Jindal et al. [18].

Conversely, Fig. 4(b) indicates that reinforcement decreases from 6.8 mm to 6.1 mm as travel speed increases from 20 m/hr to 28 m/hr. This reduction occurs because higher travel speeds cause the molten metal to spread over a larger length, leading to decreased reinforcement [19].

Fig. 4(c) further demonstrates that reinforcement decreases with increasing arc voltage. A higher arc voltage leads to an increased arc gap, causing the arc to disperse over a larger surface area. Consequently, the molten metal is distributed more widely, reducing reinforcement.Lastly, Fig. 4(d) shows that NPD has only a marginal impact on reinforcement.

These findings underscore the critical role of welding parameters in controlling reinforcement, which is crucial desired weld quality.

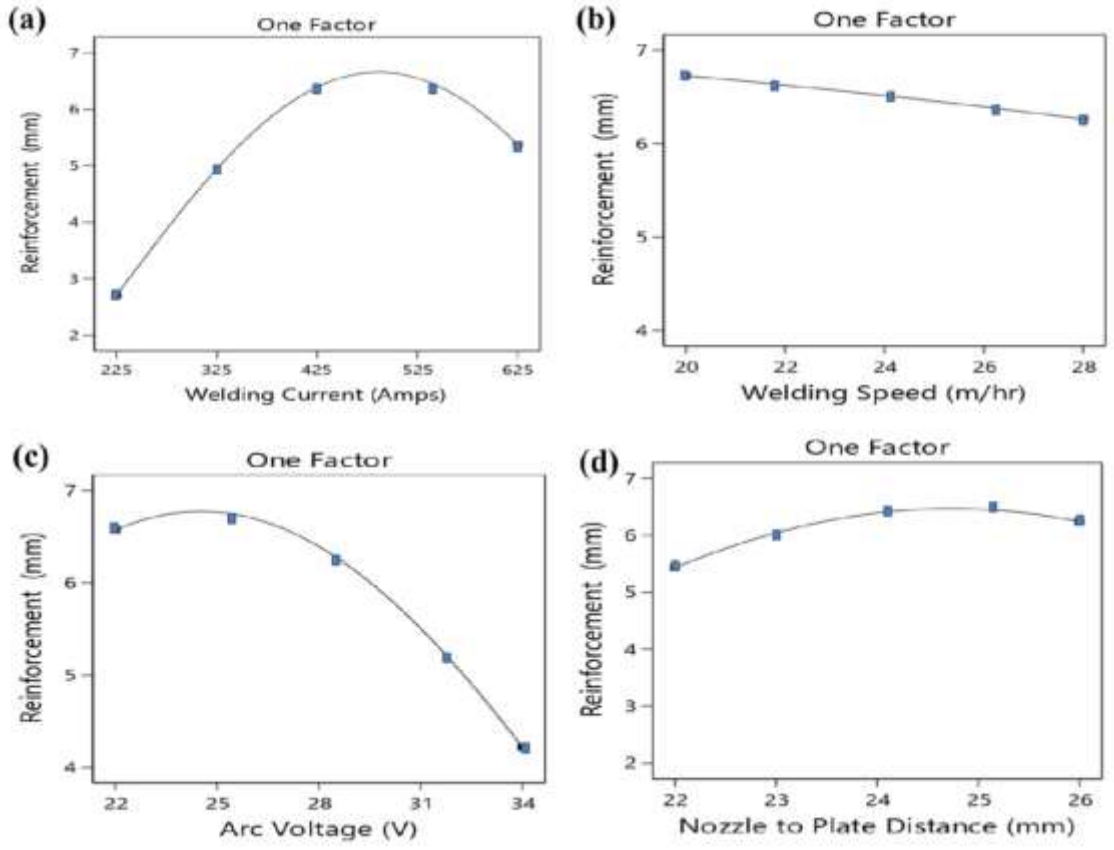

Figure 4:Effect of (a) welding current (b) welding speed (c) welding voltage (d) NPD onreinforcement

3.2 Interactive effect on weld profile

3.2.1 Interactive effects on penetration

The interactive effects of input variableonpenetration is shown in Fig. 5 (a and b). Fig. 5(a) reveals that at low travel speed (18 m/h), increasing welding current from 225 to 625 A, penetration leads to a rapid and substantial increase.In contrast, at higher travel speed particularly at 34 m/h, penetration exhibits a less gradual increase as the current is increased from low to high.

The low travel speed (18 m/h) combined with high wire current (625 Amperes) increases arc force resulting digging arc, enhancing penetration depth to 9.95 mm.

Conversely, higher travel speeds (34 m/h) and lower current (225 Amperes) reduce penetration depth to 3.43 mm. This highlights the critical interplay between travel speed and wire current in determining penetration.Fig. 5(b) shows that penetration varies with current and voltage. At high voltage (34V), penetration increases rapidly with welding current, while at low arc voltage (22V), it increases steadily. These results are supported by the findings of [20], where they found higher penetration at higher values of welding current.

3.2.2 Inter active effects on width

Fig. 5(c) illustrates the interaction between welding voltage and current on weld bead width. At low currents 225 Amperes, width increases with increase in voltage, whereas high currents 625 Amperes yield a more gradual increase. This is probably due to spreading of arc with increased voltage. The maximum width is achieved at 225 amperes and 34 V, due to the wider arc as explained above. Conversely, at low level of arc volatage (22 V), rise in current expands the molten pool, augmenting width. These findings align with [21].

Fig. 5(d) reveals a significant relationship between traval speed, voltage, and width. As welding speed increases, width decreases sharply at high voltages (34V) and gradually at lower voltages 22V. This is attributed to reduced heat energy transfer at higher speeds, resulting in smaller weld beads. Conversely, lower speeds produce wider, flatter welds due to increased heat input. Optimal width control is achieved by balancing voltage and speed, with higher voltage and lower speed yielding broader welds (27mm) and lower voltage and higher speed resulting in narrower welds (7mm).

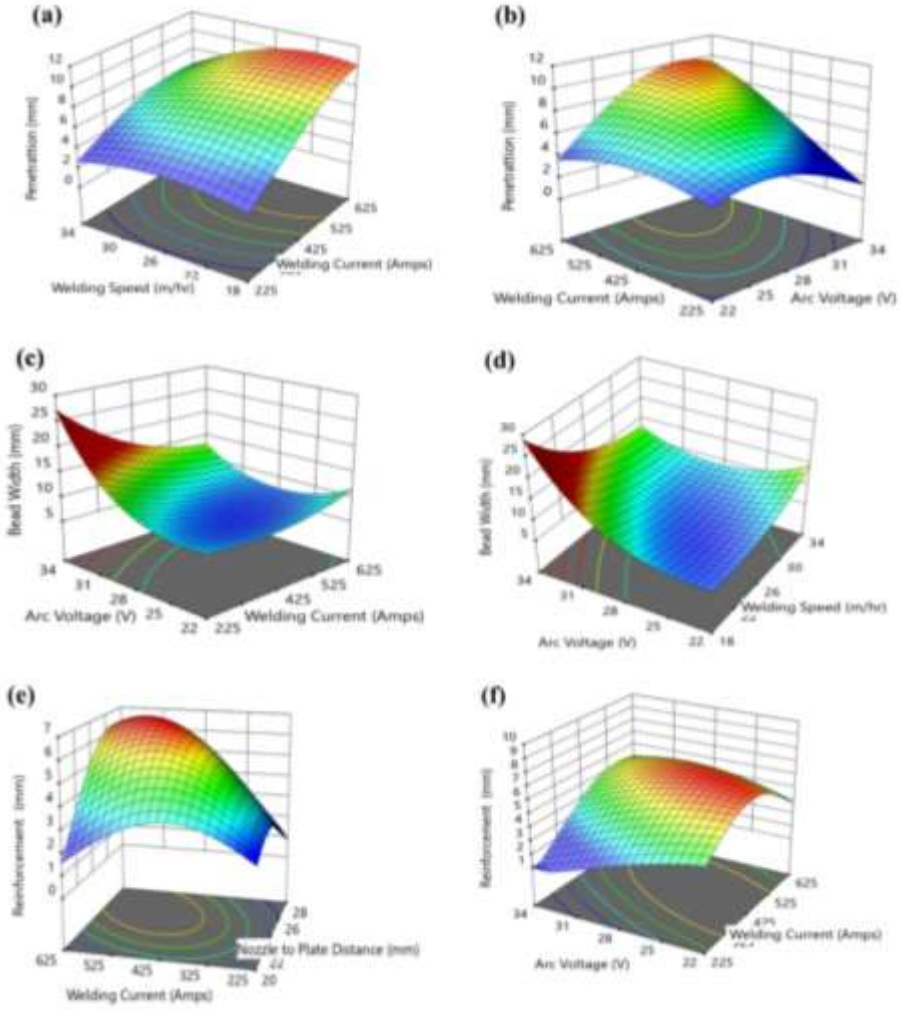

Figure 5: Interactive effect on penetration (a) current and speed (b) current and voltage. Interactive effect on bead width (c) current and voltage (d) Speed and voltage. Interactive effect on reinforcement of (e) current and NPD (f) current and Voltage

3.2.3 Interactive effects on reinforcement

Fig. 5(e) demonstrates the combined effects current and NPD on reinforcement**.** At high NPD (28 mm), increased current rapidly boosts reinforcement, because enhanced melting of wire electrode and metal deposition.

Atlower NPD (20 mm), results in a slower increase in reinforcement with higher welding current, due to a stronger arc digging action. In contrast, combining high welding current (625 amperes) with a higher NPD (28 mm) provided maximum reinforcement value (6.92 mm)

Figure 5(f) demonstrates increasing trend of reinforcement when welding current increased from 225 to 625 amperes. The lowest reinforcement value (1.90 mm) occurred at 225 Amperes and 34 V, attributed to reduced current density, slower filler wire melting, and fewer molten droplets. Conversely, higher welding current 625 amperes and lower voltage 22 V yielded a higher value of reinforcement. Notably, reinforcement increases sharply with welding current at high voltage (34 V), may be due to increased metal deposition rate.

3.3 Optimization and validation of welding parameters

The optimization of welding parameters using RSM was aimed at achieving desirable cladding characteristics by minimizing penetration and maximizing bead width. The optimized parameters obtained (current: 427 A, voltage: 30 V, welding speed: 34 m/h, and NPD: 26 mm) were validated through an experimental trial, and the predicted values were compared with the actual experimental results. The comparison, as presented in Table 6, demonstrates a strong correlation between predicted and experimental values, with minimal deviations. The percentage errors for penetration, width of weld, and reinforcement were 1.3%, 0.9%, and 2.7%, respectively. These small variations indicate that the RSM model is highly accurate in predicting welding parameters and their effects on weld bead geometry, confirming its reliability for optimization.

Among the three parameters, the highest deviation of 2.7% was observed in reinforcement, which could be attributed to slight variations in arc stability, heat input fluctuations, or material properties. However, this level of error remains within an acceptable range for practical applications. The smallest deviation of 0.9% in bead width suggests that the model provides an excellent prediction of the lateral spread of the molten metal during welding, which is crucial for achieving uniform cladding layers with minimal defects. Overall, the results validate the effectiveness of the RSM-based optimization approach in predicting and improving the welding process. The high degree of agreement between predicted and experimental values confirms the robustness of the the model, making it a valuable tool for optimizing welding parameters in cladding applications.

Table 6: Percentage error between predicted and experimental values

Method	Current(A)	Voltage(Volts)	Welding speed (m/h)	NPD(mm)		Penetration	width	reinforcement
Desirability	427	30	34	26	Predicted	5.32	15.26	4.09
	427	30	34	26	Validation test	5.25	15.11	3.98
					% error	1.3 %	0.9 %	2.7 %

3.3.1 Comparison of bead profile prepared using recycled slag and fresh flux

The bead profile obtained using recycled slag and fresh flux under optimized welding parameters is shown in Fig. 6(a, b).

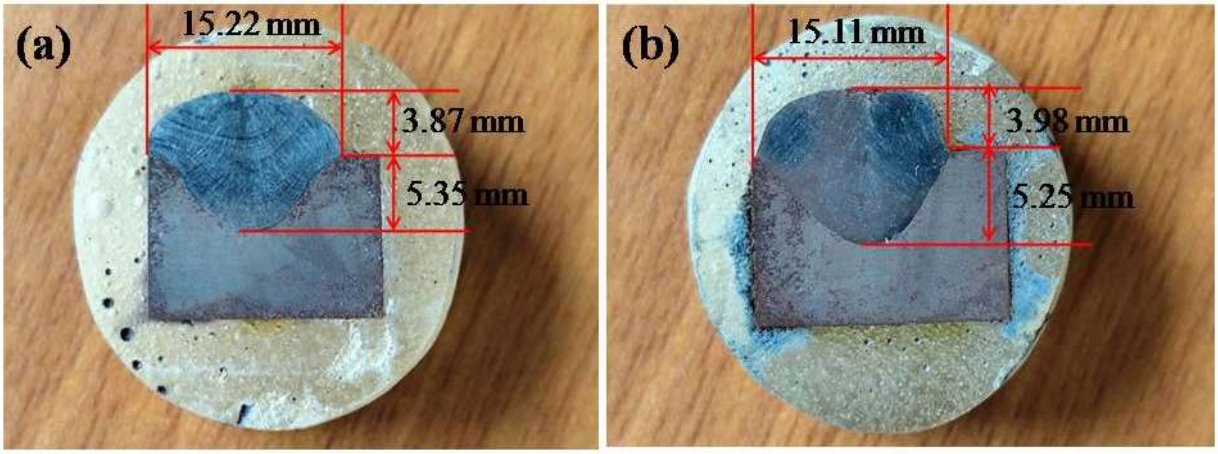

Figure 6: Bead dimensions with (a) Fresh flux, (b) recycled steel slag

A comparison of the two bead profiles indicates that the welds obtained with recycled slag closely resembles that obtained with fresh flux, suggesting that recycled slag can be effectively utilized to achieve an acceptable bead profile. The bead dimensions i.e. p, w and r of weld prepare with recycled slag are 5.25, 15.11, and 3.98 mm, respectively, whereas the corresponding values for the weld produced with fresh flux are 5.35 mm, 15.22 mm, and 3.87 mm as shown in Table 7.

Table 7: Comparison of bead profile (recycled slag and fresh flux)

	Penetration(mm)	Width (mm)	Reinforcement(mm)
Fresh flux	5.35	15.22	3.87
Developed flux	5.25	15.11	3.98

The calculated percentage errors between the two cases were 1.8% for penetration, 0.7% for bead width, and 0.1% for reinforcement, indicating minimal variation. The small differences in bead geometry suggest that the use of recycled steel slag does not significantly impact weld quality. The slightly higher deviation in penetration may be due to minor differences in the slag's thermal properties or composition, but it remains within an acceptable range for practical applications. The negligible variation in bead width and reinforcement further confirms that recycled slag can serve as a viable alternative to fresh flux in welding processes, offering a sustainable and cost-effective solution without compromising bead quality.

3.4 Microstructure and phase Analysis

The microstructural characteristics of stainless-steel claddings deposited using the submerged arc welding (SAW) process play a critical role in determining their mechanical properties and corrosion resistance. The SEM images presented in Fig. 7(a) and 8(b) provide a comparative analysis of the microstructures obtained using fresh flux and recycled slag. In both cases, the microstructure consists of a combination of skeletal delta ferrite and an austenitic matrix, which is characteristic of stainless steel welds solidifying in a ferrite-austenite (FA) mode [22]. This solidification pattern is beneficial as it helps in reducing susceptibility to solidification cracking, while maintaining an optimal balance of strength, ductility, and corrosion resistance.

The skeletal delta ferrite phase observed in the microstructure is crucial for enhancing hot cracking resistance during solidification. It also improves stress distribution and contributes to the overall toughness of the cladding layer. The presence of austenite as the primary matrix phase ensures the required corrosion resistance, particularly in aggressive environments. Since both claddings those fabricated using fresh flux and recycled slag exhibit a similar microstructural arrangement, it can be inferred that the use of recycled slag as a flux alternative does not significantly alter the fundamental solidification behavior. The comparable microstructure suggests that recycled slag can be a viable substitute for fresh flux in SAW cladding applications without compromising microstructural integrity.

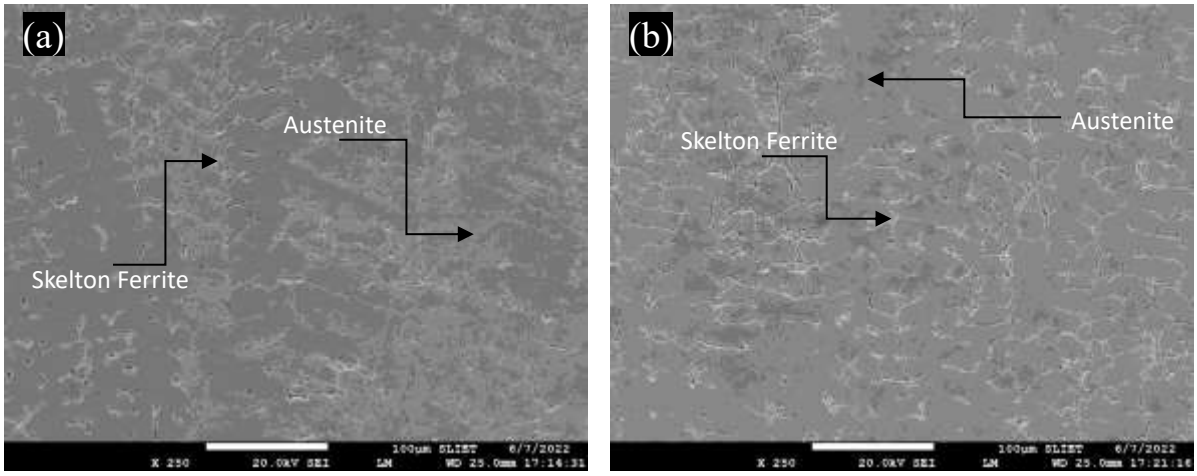

Figure 7: SEM micrograph for (a) fresh flux (b) developed flux

Overall, the results reinforce that recycled slag can be effectively utilized in the SAW process to produce high-quality stainless steel claddings. This provides a sustainable and cost-effective solution for industrial applications while ensuring the desired mechanical properties and corrosion resistance required for stainless steel claddings.

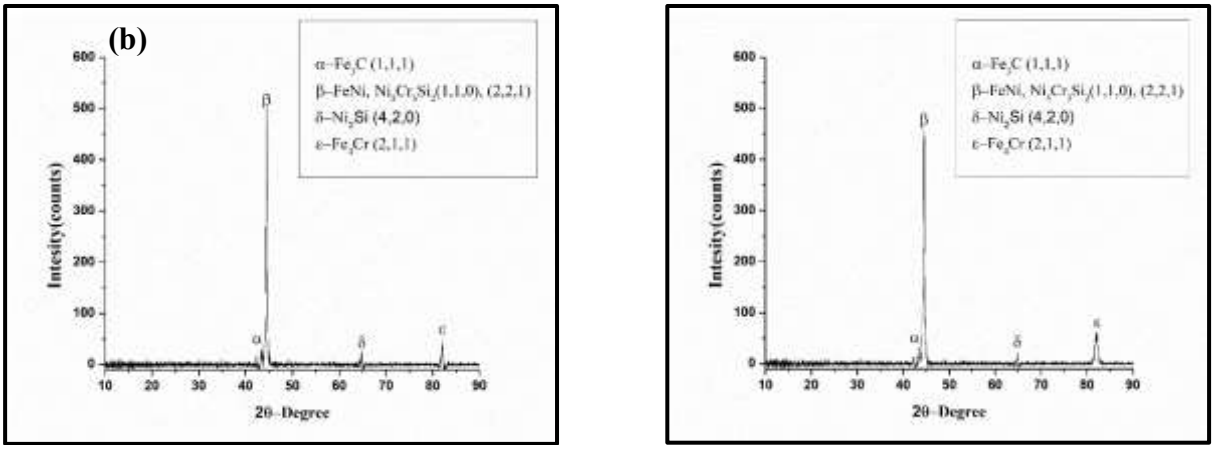

Figure 8: XRD specturm of clad layer deposited with (a) Recycled flux (b) Fresh flux

The XRD is an analytical tool, mostly used to identify the phases present in microstructure. In this technique, the obtained data is matched with known reference patterns with help of software like X-pert high score. The XRD spectrum of cladding prepared using recycled slag and fresh flux are presented in Fig. 8.

The obtained results confirmed the presence of Fe_3C, FeNi, $Ni_5Cr_3Si_2$, Ni_2Si and Fe_4Cr. The formation of Fe_3C might be due to the reaction between Fe and C present in substrate due to high heat input. The presence of FeNi, $Ni_5Cr_3Si_2$, Ni_2Si and Fe_4Cr confirms the metallurgical bonding between substrate and pure flux as elements like Si, Ni and Cr were present in fresh flux and Fe was major element of substrate. The XRD spectrum of both claddings represents similar compounds present in microstructure. This observation proves that recycled slag could produce microstructure at par with that of fresh flux.

Conclusions

1. This research demonstrate that recycling of waste steel slag as a cladding flux is a viable and sustainable alternative to conventional fresh flux.
2. The experimental results confirm that weld dimensions achieved with recycled slag are; penetration 5.25 mm, width 15.11, reinforcement 3.98 mm, which are highly comparable to that of fresh flux (5.35 mm, 15.22 and 3.78 mm) respectively, with minimum variation of 1.8%, 0.7% and 0.1%.

3. Among the welding parameters investigated, welding current significantly influence penetration and reinforcement, while arc voltage has the most pronounced effect on bead width.
4. Welding speed has a negative effect on penetration and bead width. As welding speed increased from 18 to 34 m/hr, both penetration and bead width decreased, highlighting the critical role of heat input in determining weld geometry.
5. Microstructural analysis using SEM confirmed that stainless steel claddings produced with both fresh flux and recycled slag exhibited a similar ferrite-austenite structure, ensuring comparable mechanical properties and corrosion resistance
6. Central composite rotatable design technique effectively developed predictive models for weld dimensions with a 95% confidence level.
7. These findings strongly support the adoption of recycled slag as a sustainable alternative in SAW cladding applications, offering environmental and economic benefits without compromising weld quality.

References

[1] Proctor DM, Fehling KA, Shay EC, et al. Physical and chemical characteristics of blast furnace, basic oxygen furnace, and electric arc furnace steel industry slags. Environ Sci Technol. 3492000)1576–1582.

[2] Oge M, Ozkan D, Celik MB, et al. An Overview of Utilization of Blast Furnace and Steelmaking Slag in Various Applications. Mater Today Proc [Internet]. 11(2019)516–525. Available from: https://doi.org/10.1016/j.matpr.2019.01.023.

[3] Tiwari M, Bajpai DS, Dewangan DU. Steel Slag Utilization — Overview in Indian Perspective. Int J Adv Res. 4(2016)2232–2246.

[4] Liu J, Guo R. Applications of Steel Slag Powder and Steel Slag Aggregate in Ultra-High Performance Concrete.Adv. in C. Engg. 2018(2018)1-12.

[5] Ning D, Liang Y, Liu Z, et al. Impacts of Steel-Slag-Based Silicate Fertilizer on Soil Acidity and Silicon Availability and Metals-Immobilization in a Paddy Soil. PLoS One [Internet]. 11(2016). https://doi.org/10.1371/journal.pone.0168163.

[6] Pawar AB, Chaturvedi V, Patel D, et al. Evaluating the Mechanical Properties of Silico–Manganese Slag-Blended Silica Sand Molds for Foundry Applications. Trans Indian Inst Met [Internet]. 78(2025)75. Available from: https://doi.org/10.1007/s12666-024-03544-0.

[7] Sadarang J, Nayak RK, Panigrahi I. Challenges and Future Prospective of Alternative Materials to Silica Sand for Green Sand Mould Casting: A Review. Trans Indian Inst Met [Internet]. 74(2021)2939–2952. Available from: https://doi.org/10.1007/s12666-021-02370-y.

[8] Nimker D, Wattal R. Recycling of submerged arc welding slag for sustainability. Prod Manuf Res. 8(2020)182–195.

[9] Garg J, Singh K. Reuse of Slag in Stainless Steel Cladding and Its Effect on Chemistry of Cladding.J.of Env.d.& Resh.6(2012)674-680

[10] Singh J, Singh K, Garg J, et al. Reuse of Slag as Flux in Submerged arc Welding & its Effect on Chemical Composition, Bead Geometry & Microstructure of the Weld Metal. Int. J. of Sur. E. & Mater. Tech.1(2011)24–27.

[11] Saini S, Singh K. Some Feasibility Studies for Recycling of Steel Slag as a Useful Flux for Submerged Arc Welding. J Adv Manuf Syst [Internet]. 2020;19:277–289. Available from: https://doi.org/10.1142/S0219686720500146.

[12] Saini S, Singh K. Recycling of steel slag as a flux for submerged arc welding and its effects on chemistry and performance of welds. Int J Adv Manuf Technol. 114(2021)1165–1177.

[13] Goyal N, Singh K. Waste to wealth: development of cladding flux from steel slag for submerged arc welding. J Adhes Sci Technol [Internet]. :(2024)1–13. Available from: https://doi.org/10.1080/01694243.2024.2355262.

[14] Arya HK, Singh K, Saxena RK. Effect of Weld Cooling Rates on Mechanical and Metallurgical Properties of Submerged Arc Welded Pressure Vessel Steel. J Press Vessel Technol [Internet]. 140(2018) Available from: https://doi.org/10.1115/1.4040274.

[15] Shakya P, Singh K, Arya HK. Influence of dual axial magnetic field and welding parameters on weld

characteristics in GTAW process. J Adhes Sci Technol [Internet]. :(2024)1–19. Available from: https://doi.org/10.1080/01694243.2024.2385570.

[16] Roshan R, Kumar Naik A, Kumar Saxena K, et al. Effect of welding speed and wire feed rate on arc characteristics, weld bead and microstructure in standard and pulsed gas metal arc welding. J Adhes Sci Technol [Internet]. 37(2023)3297–3314. Available from: https://doi.org/10.1080/01694243.2023.2192314.

[17] Raj P, Gill JS. Characterisation of weld bead and microhardness of SS316L weld overlays on S355J2+N steel using GTAW under E-type magnet. Eng Res Express [Internet]. 5(2023)45039. Available from: https://dx.doi.org/10.1088/2631-8695/ad058c.

[18] Jindal S, Chhibber R, Mehta NP. Investigation on flux design for submerged arc welding of high-strength low-alloy steel. Proc Inst Mech Eng Part B J Eng Manuf. 227(2013)383–395.

[19] Nouri M, Abdollah-Zadeh A, Malek F. Effect of welding parameters on dilution and weld bead geometry in cladding. J Mater Sci Technol. 23(2007)817–822.

[20] Kumar M, Singh J, Singh Uppal A. Improvement in corrosion resistance of AISI 316L stainless steel weld cladding using GTA remelting technique. Mater Today Proc [Internet]. 265(022;6)3224–3228. Available from: https://www.sciencedirect.com/science/article/pii/S2214785322036744.

[21] Choudhary S, Shandley R, Kumar A. Optimization of agglomerated fluxes in submerged arc welding. Mater Today Proc [Internet]. 5(2018)5049–5057. Available from: https://doi.org/10.1016/j.matpr.2017.12.083.

[22] Dillon CP. Corrosion resistance of stainless steels. CRC Press; 1995.